Fibers and Polymers 2001, Vol.2, No.2, 98-107

Synchrotron SAXS Study on the Micro-Phase Separation Kinetics of Segmented Block Copolymer

Han Sup Lee*, So Ra Yoo[1], and Seung Won Seo[1]

Department of Textile Engineering, Inha University, 253 Younghyun-dong, Incheon 402-751, Korea
[1]R & D Center for Fibers and Textiles, Hyosung Co., 183 Hoge-Dong, Dongan-gu, Anyang 430-080, Korea
(Received November 6, 2000; Revised April 27, 2001; Accepted May 4, 2001)

Abstract: The phase transition behavior and isothermal micro-phase separation kinetics of polyester-based thermoplastic elastomer were studied using the synchrotron X-ray scattering (SAXS) method. The structural changes occurring during heating period were investigated by determining the changes of the one-dimensional correlation function, interfacial thickness and Porod constant. Based on the abrupt increases of the domain spacing and interfacial thickness, a major structural change occurring well below the melting transition temperature is suggested. Those changes are explained in terms of melting of the thermodynamically unstable hard domains or/and the interdiffusion of the hard and soft segments in the interfacial regions. SAXS profile changes during the micro-phase separation process were also clearly observed at various temperatures and the separation rate was found to be sensitively affected by the temperature. The peak position of maximum scattering intensity stayed constant during the entire course of the phase separation process. The scattering data during the isothermal phase separation process was interpreted with the Cahn-Hilliard diffusion equation. The experimental data obtained during the early stage of the phase separation seems to satisfy the Cahn-Hilliard spinodal mechanism. The transition temperature obtained from the extrapolation of the diffusion coefficient to zero value turned out to be about 147± 2°C, which is close to the order-disorder transition temperature obtained from the Porod analysis. The transition temperature was also estimated from the invariant growth rate. By extrapolating the invariant growth rate to zero, a transition temperature of about 145± 2°C was obtained.

Keywords: Microphase separation, Kinetics, Thermoplastic elastomer, Synchrotron SAXS

Introduction

A polymeric chain of thermoplastic elastomer (TPE) consists of two chemically distinct segments, i.e., hard and soft segments. Due to the thermodynamic incompatibility between the two segments, it undergoes a microphase separation process resulting in the phase-separated, heterogeneous structure of hard and soft domains[1-3]. Since the glass transition temperature of hard domains, of which the major component is hard segment, is well above the room temperature, a hard domain acts as a physical crosslinking. The soft segments are in the rubbery state at room temperature due to its low glass transition temperature. Thus if external stress is applied, the soft segments in the soft domain can be extended rendering high elongation of the TPE. The extended soft segment can relax to its undeformed state due to the entropically driven retractile force when the external stress is released. Since both ends of soft segment are chemically connected to the hard segments, which are generally anchored to the glassy hard domains, plastic deformation is limited and the elastic recovery can be achieved for the TPE[1,3-5].

The physical properties of TPE are determined by many factors, such as chemical nature and composition of both segments, phase separated structure, and degree of phase separation[4]. During processing, the TPE is generally heated above the order-disorder transition temperature (T_{ODT}) to achieve a homogeneous and low viscosity state. After the overall shape of TPE is formed, the temperature is lowered below T_{ODT} to solidify the shape. Upon cooling, the micro-phase separation process starts to turn the homogeneous state into the phase separated heterogeneous state. Since the physical properties of TPE are sensitively affected by the phase separated structure which is determined by the phase separation process, the phase separation behavior, including phase separation kinetics, has been widely studied using various methods, such as thermal, spectroscopic and scattering methods, in order to establish the structure-property relationship.

Phase separation kinetics of polymer blends and simple block copolymers has been widely studied experimentally as well as theoretically[6-14]. However, microphase separation kinetics of segmented block copolymers has not been studied extensively, mainly due to the complexity of the structure and the lack of concrete theoretical development. Polymer blends or simple block copolymers, such as diblock or triblock copolymers, undergo phase separation through spinodal decomposition or nucleation and growth mechanisms, depending on the composition of the constituent of the chain and the phase separation temperature. Even though the phase-separated structure of polymer blends may be eventually similar, irrespective of the phase separation mechanisms, the initial phase separation process is distinctively different.

Phase separation kinetics have been generally studied with various scattering methods using light[7,10,12], x-ray[8,9, 13,15-18], and neutron[12,14] sources, even though other methods, such as thermal and spectroscopic methods[19-

*Corresponding author: hslee@inha.ac.kr

23], were successively applied to monitor the process. The domain size of the segmented block copolymers is generally in the range of 100-500 Å which can be easily studied using the small angle x-ray scattering method[11]. There are two major factors limiting the SAXS method for the study of the microphase separation kinetics of the TPE. Even though complete phase separation may be achieved after several days, the majority of the phase separation occurs within several minutes during the processing of TPE. Special method is therefore required to follow the fast changing process. And, the electron density difference between the two domains of TPE is relatively low, resulting in very low scattering intensity. The low contrast problem is significant, especially during the early stage of phase separation. Both problems can be overcome by using a high energy x-ray source, such as synchrotron radiation.

Synchrotron x-ray radiation has been reported to be successfully used for the study of the micro-phase separation kinetics of thermoplastic elastomers[11,16,18]. Chu and coworkers studied phase separation kinetics of polyurethanes [16,18]. They found that phase separation rate depends strongly on the annealing temperature. For the polyurethanes consisting of 4,4'-diphenylmethane diisocyanate (MDI), 1,4-butane diol (hard segment content is about 50 wt%) and poly(tetramethylene oxide) endcapped with poly(propylene oxide) (soft segment, Mn≒1000), the maximum phase separation rate was observed at around 80-107°C. The rate decreased with the increase of temperature due to increased compatibility at higher temperatures. They also studied the effect of soft segment length and structure on the microphase separation kinetics of polyurethanes. The micro-phase separation kinetics were interpreted in terms of a relaxation process having single or double relaxation times, depending on the chemical structure of the soft segment. It was also reported that the relaxation time was sensitively affected by the soft segment molecular weight. By increasing the soft segment molecular weight from 1000 to 2000 g/mol, the relaxation time was reduced from about 10^3 to 64 sec. They concluded that three factors which control the micro-phase separation rate of segmented polyurethanes are hard segment mobility, system viscosity, and hard segment interactions. Even though the micro-phase separation process of segmented polyurethane was clearly observed and analyzed in terms of a relaxation process, the overall intensity and signal to noise ratio was relatively low due to the inherently low electron density contrast between the hard and soft domains, thus preventing a more quantitative analysis.

In this study, micro-phase separation kinetics of a polyester-based thermoplastic elastomer was studied using synchrotron x-ray radiation. The elastomer was heated above its order-disorder transition temperature to ensure a homogeneous state, and then quenched to various phase separation temperatures to induce a heterogeneous phase separated state. SAXS profile changes during the micro-phase separation process were clearly observed with high signal to noise ratio, and experimental observations during the initial micro-phase separation process were tested according to the Cahn-Hilliard linearization theory[9,10,24-27].

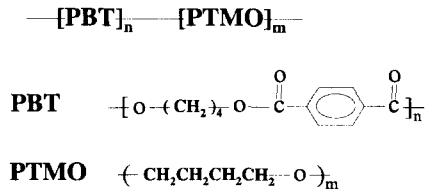

Figure 1. Approximate chemical structure of the sample used in this study. Small amount (about 4%) of aromatic chain extender is included in addition to the butanediol to lower the melting temperature of the hard segments.

Experimental Section

Material

The polyester-based segmented block copolymer, Esrel 1040M®, of which the approximate chemical structure is shown in Figure 1 was supplied by the Cheil Synthetic Inc. (Gi-heung, Korea). The hard segment consists of poly (butylene terephthalate) and 1,4-butanediol (hard segment content is 43.8 wt%), and the soft segment is poly (tetramethylene oxide). It contains a small amount (about 4%) of aromatic chain extender in addition to butanediol. Due to the additional chain extender, it showed a melting temperature of 150°C, which is well below the melting temperature of poly(butylene terephthalate).

Instrumentation

Synchrotron SAXS measurement was carried out at the beam line 3C2, Pohang Light Source (Pohang, Korea). Details about the beam line have been described elsewhere[28]. The monochromatic light of 1.5988 Å wavelength was obtained with the Si(111) double crystal monochromator. A one-dimensional diode array detector was used. The temperature jumping stage used in this study consists of two metal blocks of high thermal mass[16,18,29]. The temperature of first block was maintained at 200°C, which is well above the melting temperature of Esrel 1040 M, and temperature of second block was adjusted to the isothermal phase separation temperature. For the phase separation kinetic study, the sample was initially stored in the first metal block for three minutes, which was long enough to ensure a homogeneous state. The micro-phase separation process started by bringing the sample from the first to second metal block using a pneumatic pressure device. It took 1.5 to 2 minutes to change the sample temperature from 200°C to within few degrees of the isothermal phase separation temperature. For most of temperatures studied, the structural change occurring during this quenching process was observed to be negligible. In order to obtain the scattering only from the sample,

routine corrections such as sample attenuation, parasitic and background scattering, and incident intensity fluctuation were performed.

Results and Discussion

Structural Changes During Heating

Figure 2 shows synchrotron SAXS profiles obtained during the heating period. The scattering intensity is plotted with respect to the scattering vector q which is defined below.

$$q = \frac{4\pi}{\lambda}\sin\theta \tag{1}$$

Here, 2θ is the scattering angle. Temperature was increased slowly (about 5°C/min) to each measuring temperature and maintained at that temperature while the scattering data was being collected. The SAXS profile which was obtained at room temperature (not shown in Figure 2) was almost identical to that obtained at 50°C. It is clear that the material has a phase-separated structure at room temperature. As temperature increases, the scattering peak maximum decreases and eventually disappears at about 150°C, indicating that order-disorder transition occurs at that temperature. Even though order-disorder transition occurs at about 150°C, the scattering intensity starts to decrease at about 100°C. This result indicates that internal structural changes occur well below the melting transition.

The transition temperature and domain spacing can be directly obtained from the correlation function. Since this material is expected to have lamellar type hard domains, the electron density correlation will be observed only along the one-dimensional direction perpendicular to the lamella plane [16,18,30]. One-dimensional correlation function is defined below[31].

$$\gamma_1(r) = \frac{\int_0^\infty q^2 I(q)\cos(qr)dq}{\int_0^\infty q^2 I(q)dq} \tag{2}$$

The correlation functions obtained at four different temperatures are shown in Figure 3. The periodic pattern is clearly observed at two lower temperatures. The D-spacing obtained from the correlation function at 25°C is about 143 Å, and its value increases with the temperature. As shown in Figure 2, the first maximum point is not obvious for the correlation function obtained at 160°C, which is well above the melting temperature of the sample.

The order-disorder transition behavior is better observed from the Porod analysis of the scattering data. If the electron density profile at the interface between the hard and soft domain is approximated with the linearly decreasing function from the electron density of hard domain to that of soft domain, the intensity at the high q value can be related to the interface thickness E as shown in equation (3).

$$\lim_{q\to\infty} I(q) = \frac{K_p}{q^4}\left(1 - \frac{E^2q^2}{12}\right) \tag{3}$$

$$K_p = 2\pi(\Delta\rho)^2 S \tag{4}$$

Here, K_p in equation (4) is the Porod constant, $\Delta\rho$ is the electron density difference between the hard and soft domains, and S is total interfacial area. By plotting $I(q)q^4$ against the q^2 at the high q value, the interfacial thickness E and Porod constant K_p can be obtained from the slope and intercept, respectively. In Figure 4, the Porod constant and interfacial thickness are plotted as functions of temperature.

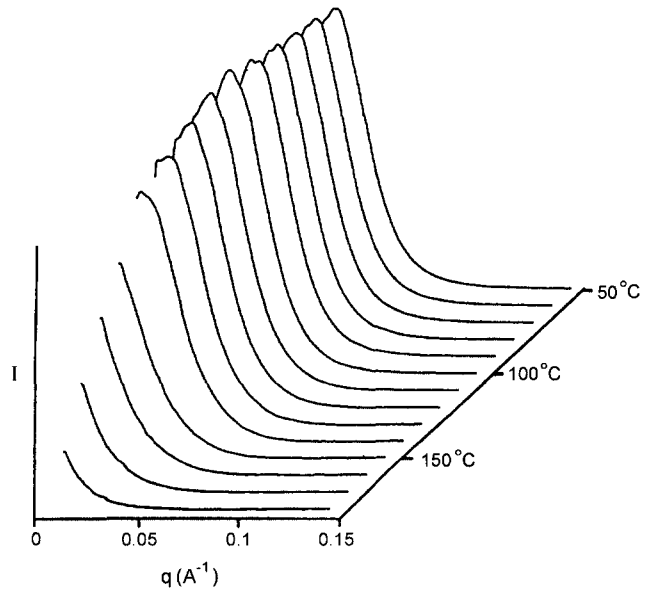

Figure 2. SAXS profiles obtained at various temperatures during heating period. Temperature for each corresponding profile is also denoted. Profile at room temperature (not shown above) is practically identical to that at 50°C.

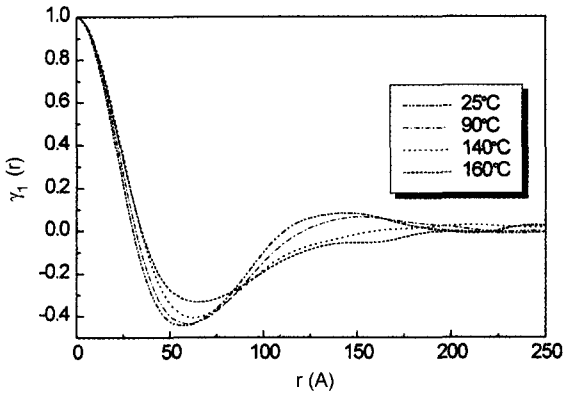

Figure 3. One dimensional correlation functions of the four SAXS profiles obtained during heating period. Temperature of each function is denoted in the inset.

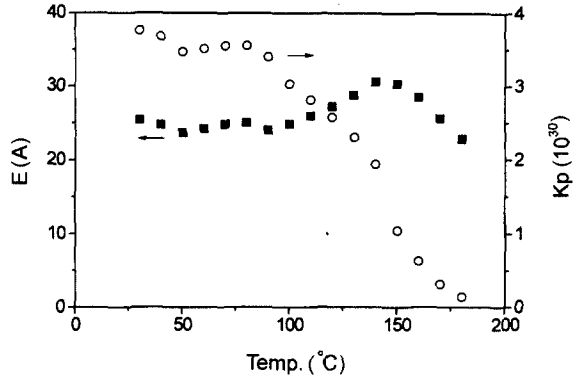

Figure 4. Interface thickness(left ordinate in Å) and Porod constant (right ordinate in counts $Å^{-4}$) as a function of temperature during heating period.

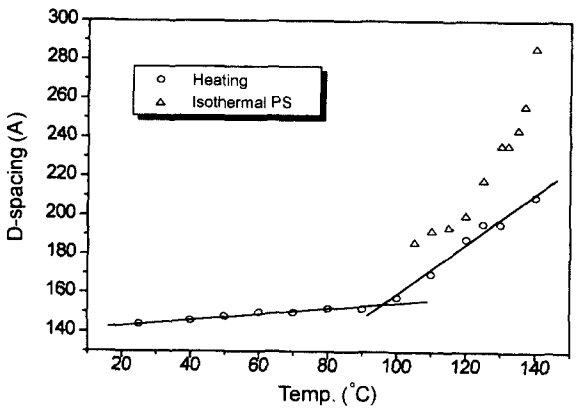

Figure 5. Domain spacing obtained during heating period (in circle) and after isothermal micro-phase separation (in triangle).

When the sample starts to melt, hard segments initially contained in the hard domain will diffuse out into the soft matrix resulting in a decreased $\Delta\rho$ and S. According to Figure 4, the Porod constant starts to decrease at about 90°C, which is well below the melting transition point. As expected, the maximum decrease rate was observed at about 150°C. This result indicates that the structural change starts at about 90°C. It may be due to the melting of the thermodynamically unstable small domains, even though the stable large-size domains melt eventually at the thermodynamic melting temperature, i.e., 150°C. The structural changes that occur below the melting temperature can be also inferred from the interfacial thickness data. Above the melting temperature, the scattering data can not be approximated with equation (3), which is applicable to the three phase model. Therefore, the interfacial thickness data above 150°C in Figure 4 should not be considered as absolute values. However, the abrupt decrease of the interfacial thickness at 150°C clearly corresponds to the melting transition point of the sample. It is to be noted that the interfacial thickness starts to increase at about 90°C, at which temperature the Porod constant starts to decrease. Increase of interfacial thickness indicates the broadening of the interface. As the temperature increases above 90°C, the mobility of the hard segments, especially in the noncrystalline hard domains, will be increased. Also the compatibility between hard segments and soft segments increases, facilitating the diffusion of the hard segments in the hard domains into the interfacial region.

Structural changes occurring well below the melting transition point can be also observed from the D-spacing values obtained at different temperatures. In Figure 5, D-spacing obtained from Figure 3 is plotted as a function of temperature. As explained above, the D-spacing is obtained only at temperatures below 150°C. Below 90°C, the D-spacing value increases slowly with the temperature, possibly due to the thermal expansion of the domains. The rate of increase changes abruptly at about 90°C, indicating once again the structural change which begins at this temperature. This result is consistent with those shown in Figure 4. Whether the structural change occurring at this temperature is due to the interdiffusion of the hard and soft segments in the interfacial region is not clear at this stage. If the interdiffusion of the segments is the only mechanism occurring in this temperature range, the D-spacing may not be affected significantly. Therefore, structural changes occurring above 90°C may result from the melting of the unstable small-size hard domains as well as the interdiffusion of the segments in the interfacial region. Additional experimentation would be required to establish a more concrete conclusion regarding the structural change mechanism operating in this temperature range.

The data points marked with triangles in Figure 5 were obtained from isothermal micro-phase separation experiments. The D-spacing from the isothermal phase-separation experiment is greater than the corresponding D-spacing values obtained from the heating experiment. This fact indicates that the domain structure obtained from the isothermal micro-phase separation is different from the domain structure obtained at the corresponding temperature during the heating experiment. For the isothermal micro-phase separation, not all hard segments can phase-separate into the hard domains. There is critical hard segment length at any given iso-thermal phase separation temperature. Hard segments longer than the critical length can phase-separate into the hard domains, whereas shorter hard segments will remain in the soft matrix. Since only hard segments longer than the critical length form hard domains, the D-spacing of the phase separated structure in the isothermal phase-separation experiment will be greater than the corresponding D-spacing in the heating experiment.

Isothermal Micro-phase Separation Kinetics

Synchrotron SAXS profiles obtained during four different

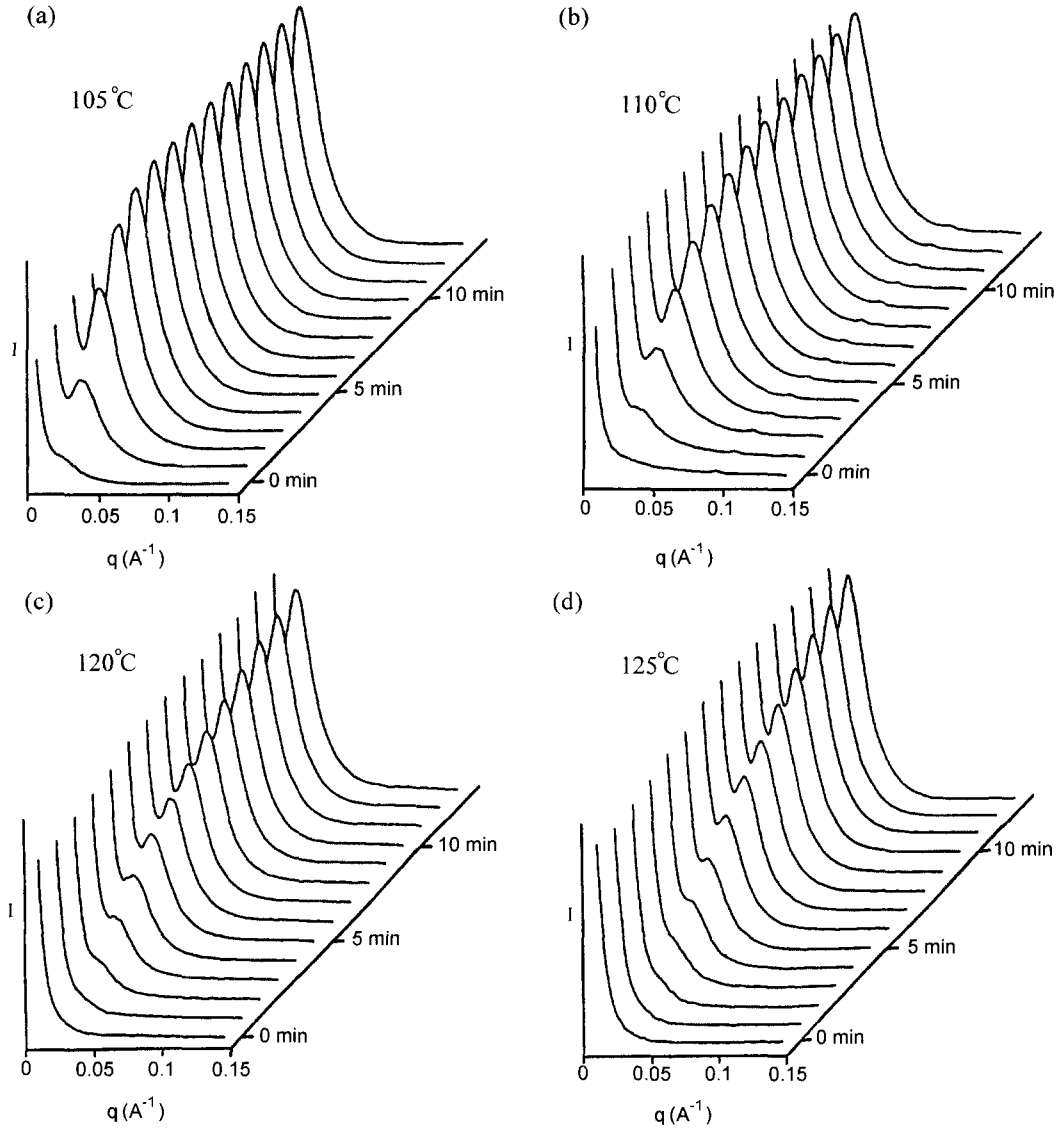

Figure 6. SAXS profiles obtained during isothermal micro-phase separation process at (a)105°C, (b)110°C, (c) 120°C, (d) 125°C. Sample was exposed to incident X-ray for 60 sec. to collect each profile. The time denoted above corresponds to the initiation time of 60 seconds exposure.

isothermal phase separation temperatures are shown in Figure 6. The profiles obtained at the zero phase-separation times shown in Figure 6(b,c,d) show a monotonic decrease of the scattering intensity, which is indicative of the homogeneous phase-mixed state. As phase-separation time increases, the scattering maximum starts to show up, and its intensity increases gradually. By comparing the four sets of data in Figure 6, it is easily concluded that the phase-separation rate is sensitively affected by the phase-separation temperature. The phase-separation rate at 120°C, for example, is much smaller than that at 105°C. It is to be noted that the exposure time for each profile was 60 sec. Therefore, each profile represents the average structure during a one minute interval. Even though this inherent averaging process will be insignificant for the slow phase-separation process, its effect can be somewhat significant for phase separations at lower temperatures. The scattering profile observed just after quenching to 105°C (Figure 6(a)) shows small scattering intensity in addition to that of homogeneous state. This may be due to the phase-separation during the first one-minute period, and/or phase-separation during the approximate two minutes quenching period. The phase-separation of the zero phase separation time at temperatures above 105°C seems to be minimal, as observed from the first scattering profiles in each set of data shown in Figure 6.

D-spacings obtained from the scattering peak maximum during isothermal phase-separation are shown in Figure 7. It is clear that the scattering peak maximum stays constant

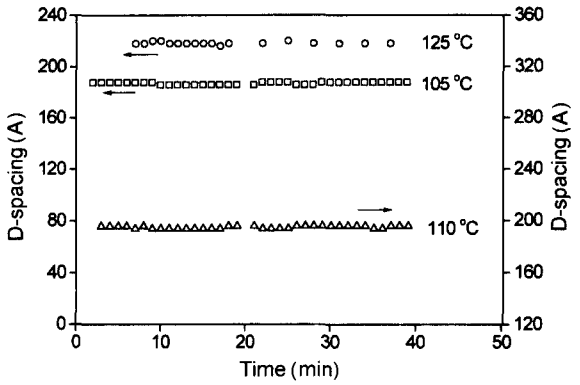

Figure 7. Domain spacing as a function of time during the isothermal micro-phase separation process at three temperatures. Two ordinates are used to avoid the congestion of the data.

during entire course of the micro-phase-separation process studied. For the micro-phase separation of simple block copolymers, the micro-phase separation is known to involve at least three stages[8,9,29]. Initially, concentration fluctuation is established, and its amplitude grows with time. The scattering peak maximum stays constant during this initial period. If the concentration fluctuation becomes sufficiently large, the copolymer chains begin to stretch, resulting in an increase of the D-spacing. In the last stage of phase separation of simple block copolymer, coarsening of the microphases and decrease of the interfacial width occur, while the concentration fluctuation and the equilibrium period are maintained. The results shown in Figure 7 indicate that the micro-phase separation of segmented block copolymer is very different from that of simple block copolymer. Whereas diblock copolymers have only one junction point on each block, both ends of each segment in the segmented block copolymers are chemically linked to other segments. Therefore, the chain connectivity effect will be much more significant for segmented block copolymers. The constant position of maximum scattering intensity has also been observed with polyurethanes, another type of segmented block copolymers. It seems to be a general characteristic of the segmented block copolymers.

It is well known that the chains of simple block copolymers in the micro-phase separated state are somewhat extended from the random conformation[8,32-34]. Since the chain connectivity of segmented block copolymers is more severe than that of simple block copolymers, the chain extension in the micro-phase separated state will be obvious. Direct evidence for the chain extension of the segmented block copolymers in the micro-phase separated state has been obtained[35]. It is noted that the scattering maximum stays constant during the entire course of the micro-phase separation process of the segmented block copolymers, even though the chains (especially flexible soft segment) have to be stretched to exist in the micro-phase separated state. This results indicates that the flexible segments in the segmented block copolymers have to be stretched even during the initial stage of phase separation. Since all segments in the chain are chemically linked, the whole chain has to be in an appropriate conformation (flexible segments have to be in an extended conformation) to take part in the concentration fluctuation. Unlike the micro-phase separation of simple block copolymers, in which the chain stretching happens only during the second stage, the chain stretching seems to persist during entire course of the micro-phase separation of segmented block copolymers. The constant scattering peak maximum observed in Figure 7 appears to support the above arguments.

For the early stage of spinodal phase separation, when the amplitude of concentration fluctuation is relatively small, the time dependence of concentration change can be expressed by the following linearized form of Cahn's diffusion equation [24,36],

$$\frac{\partial \phi}{\partial t} = M\left[\left(\frac{\partial^2 G}{\partial \phi^2}\right)\nabla^2\phi - 2K\nabla^4\phi\right] \tag{5}$$

where M is mobility, and K is interfacial energy coefficient. The general solution of equation (5) is

$$\phi(\vec{r}) - \phi_0 = \sum_{\vec{q}} \exp[R(\vec{q})t] \cdot [A(\vec{q})\cos(\vec{q}\cdot\vec{r}) + B(\vec{q})\sin(\vec{q}\cdot\vec{r})] \tag{6}$$

where ϕ_0 is the average composition and $R(q)$ is amplification factor of the fluctuation for the given q. According to equation (6), the amplitude of periodic concentration fluctuation is dependent on the exponential function of the amplification factor, $R(q)$.

$$R(q) = -Mq^2\left[\left(\frac{\partial^2 G}{\partial \phi^2}\right) + 2Kq^2\right] \tag{7}$$

Since the $R(q)$ has a sharp maximum at $q = q_{max}$,

$$q_{max} = \frac{1}{2}\left[\frac{-(\partial^2 G/\partial\phi^2)}{K}\right]^{1/2} \tag{8}$$

the spinodal phase separation is mainly dominated by the fluctuation mode having q_{max}. The scattering peak position that remains constant during the early stage of spinodal phase separation is determined by this particular fluctuation mode.

In the case of micro-phase separation of segmented block copolymers, the periodicity of concentration fluctuation will not be determined by the thermodynamic factors shown in equation (8). Since all of the segments are chemically linked by chemical bonds, the periodicity corresponding to q_{max} is inherently determined by the length of hard and soft segments. The growth of all fluctuation modes having q other than q_{max} will, therefore, be even more strictly suppressed for the micro-phase separation of segmented block copolymers. The constant scattering peak position during the entire course of the micro-phase separation

process, as shown in Figure 7, supports this argument. Even though there have been many experimental as well as theoretical developments on the micro-phase separation of simple block copolymers, the basic theory governing the micro-phase separation of segmental block copolymers has not been well developed. Therefore, it will be interesting to check whether the experimental observation shown in Figure 6 might be consistent with the theoretical predictions of equations (5) and (6).

According to the linearized Cahn-Hilliard theory[9,10,24-27], the scattering intensity at the given scattering vector during the early stage of spinodal phase separation is given by

$$I(q, t) \sim \exp[2R(q)t] \tag{9}$$

which predicts that the logarithmic scattering intensity at the given q increases linearly with time. In Figure 8, peak scattering intensity is plotted with time for the micro-phase separation at three temperatures. It is clear that the entire data set can not be expressed by a single straight line. It is to be noted that the Cahn-Hilliard theory expressed in equations (5), (6), and (9) is only applicable to the early stage of the spinodal phase separation, during which the concentration fluctuation is relatively small. Even though the scattering peak position remains constant during the whole phase separation period for this sample, it does not necessarily mean that the linear theory can be applied to the whole period. As mentioned before, the periodicity is mainly determined by the physical structure of the polymer chain, not by thermodynamic factors. A straight line may approximate the part of data shown in Figure 8, which is obtained especially during the initial stage of phase separation. The linearity is even clearer at higher temperature (130°C) at which the phase separation rate is slower and concentration fluctuation remains small for an extended period of time. From the slope of the initial linear line, the amplification factor $R(q)$ could be obtained.

In Figure 9, logarithmic scattering intensity obtained

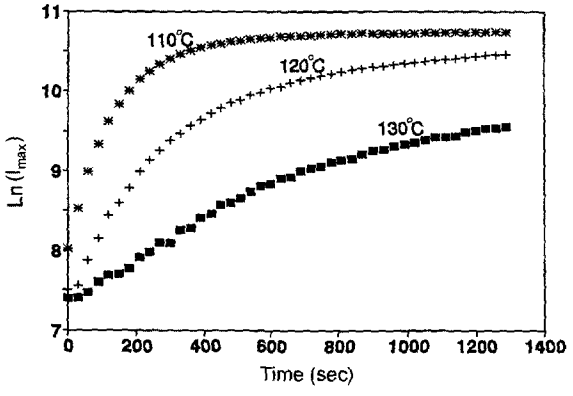

Figure 8. Logarithm of maximum scattering intensity as a function of micro-phase separation time at three temperatures.

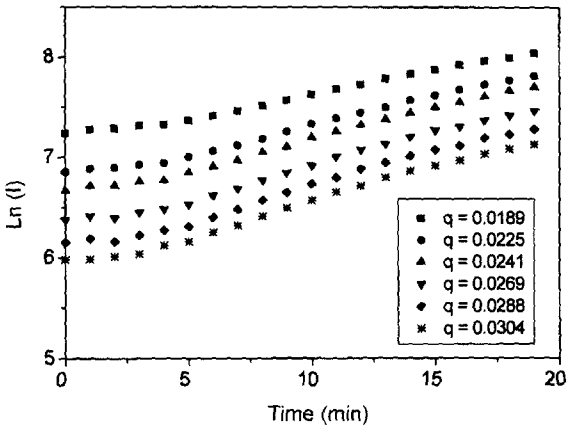

Figure 9. Logarithm of scattering intensity at the various scattering vectors.

during the micro-phase separation at 143°C is plotted as a function of the phase separation time at various q values. Whereas there was a very short induction period for the micro-phase separation at 130°C (see Figure 8), a rather longer induction period can be observed for the micro-phase separation at this higher temperature. The origin of the induction period is not clear at this moment. As mentioned previously, the chain has to be stretched to take part in the micro-phase separation process, even at the early stage of phase separation. Since most segments in a chain are expected to be included in the phase separation process at the same time, it will take some time for the whole segments to rearrange their conformation, resulting in the slowing down of phase separation kinetics. The temperature of the sample during the quenching process can not be changed as a step function. Quenching to within a few degrees of the micro-phase separation temperature took some time (1.5 to 2 min). Therefore, there might be a range of a few degrees of uncertainty in the sample temperature during the very early stage of phase separation. This effect might also contribute to the deviation from linearity. Understanding the exact nature of the initial induction period will require additional experimentation. From the linear region in Figure 9, the amplification factor $R(q)$ at various q values could be obtained.

Equation (5) becomes the same form as the Fick's diffusion equation, if the second term in the right hand side is ignored. Therefore, $M\left(\frac{\partial^2 G}{\partial \phi^2}\right)$ is defined as diffusion coefficient D, and equation (7) can be rewritten.

$$\frac{R(q)}{q^2} = -D - 2MKq^2 \tag{10}$$

Equation (10) predicts the linear relationship between $R(q)/q^2$ and q^2. In Figure 10, $R(q)/q^2$ values are plotted with respect to q^2 for five different micro-phase separation temperatures. The linear relationship appears to hold for all five temperatures. From the intercept, the diffusion coefficient

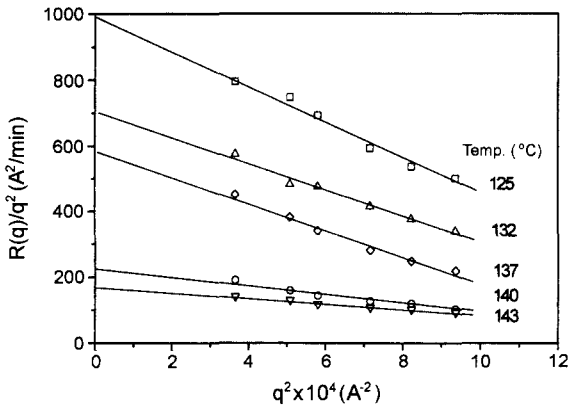

Figure 10. $R(q)/q^2$ vs q^2 at various micro-phase separation temperatures. The intercept of each straight line corresponds to the negative diffusion constant.

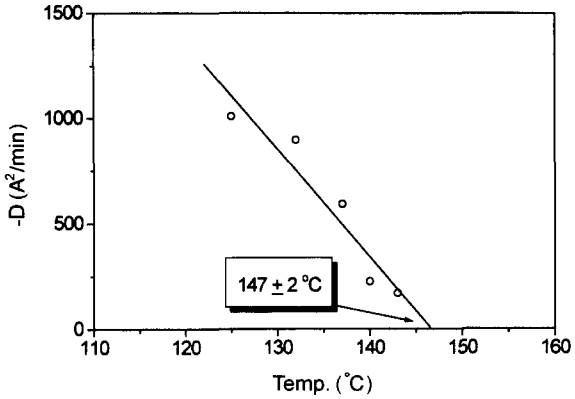

Figure 11. Negative diffusion constant obtained at various isothermal micro-phase separation temperatures.

D can be obtained. It is noted that the diffusion coefficient is negative, as expected from the spinodal phase separation mechanism.

The diffusion coefficients obtained are plotted as a function of micro-phase separation temperature in Figure 11. The absolute magnitude of the diffusion coefficient becomes smaller as the temperature increases. The diffusion coefficient becomes positive in the binodal and single phase region. Therefore, it will become zero if the spinodal line in the phase diagram is crossed. In Figure 11, the diffusion coefficient appears to become zero at 147± 2°C. The complete phase diagram of the segmented block copolymers has not been obtained. It is also not known whether the conventional phase separation mechanisms, such as nucleation and growth, and spinodal decomposition, can be directly applied to the phase separation of segmented block copolymers. Thus, the clear distinction between the spinodal and binodal point can not be made at this stage. Anyhow, the transition temperature at 147± 2°C is very close to the order-disorder transition temperature obtained from Figure 4.

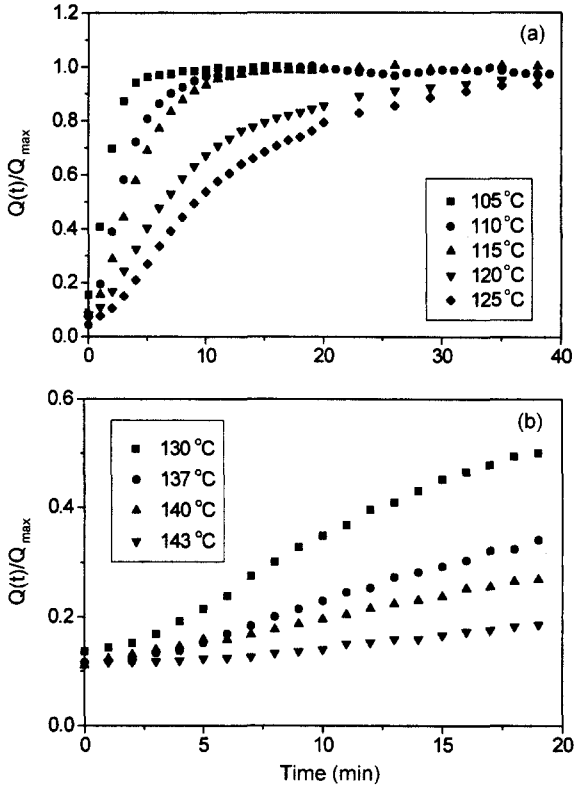

Figure 12. Relative invariant ($Q(t)/Q_{max}$) at various temperatures as a function of time. Phase separation temperatures are denoted in the Figure.

Invariant Q can be obtained from the integrated scattering intensity[31,37-39].

$$Q = \int_0^\infty I(q)q^2dq \tag{11}$$

For the two phase model with a sharp phase boundary, the invariant is related to the structure parameters,

$$Q \sim \phi_1\phi_2(\rho_1 - \rho_2)^2 \tag{12}$$

where ϕ_i and ρ_i are the volume fraction and the electron density of the i-th phase, respectively. As the amplitude of the concentration fluctuation grows during the early stage of the spinodal phase separation, the electron density contrast between the hard and soft domains increases resulting in the increase of the invariant Q. Therefore, micro-phase separation rate can also be estimated from the time dependence of the invariant value[7]. The relative invariant, $Q(t)/Q_{max}$, is shown in Figure 12(a) and (b) as a function of micro-phase separation time. The Q_{max} is the maximum invariant obtained from the isothermal micro-phase separation process. It is easily observed that the invariant growth rate decreases with the temperature. The invariant growth rate is obtained from the initial linear region of the data shown in Figure 12 and

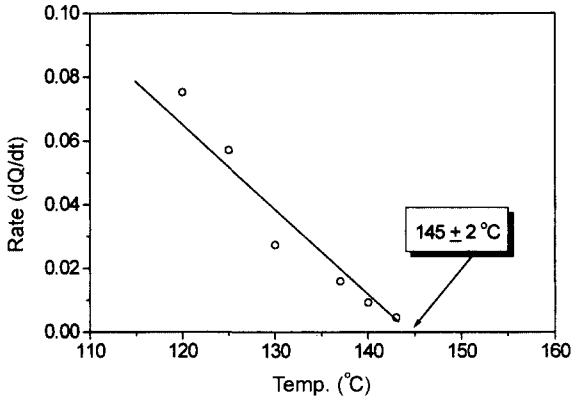

Figure 13. Initial invariant growth rate as a function of micro-phase separation temperature.

plotted in Figure 13. The functional shape of temperature dependence of the invariant growth rate is, of course, not known. Thus, an exact method for extrapolating the invariant growth rate to zero value can not be determined. However, the temperature at the zero growth rate can be estimated without significant error by using linear extrapolation, and it turns out to be about 145± 2°C. This temperature is again in relatively good agreement with the value obtained from the diffusion coefficient method (147± 2°C). This result supports the previously mentioned spinodal method of obtaining the transition temperatures for segmented block copolymers. However, without the detailed phase diagram of this type of material, the distinction between the two transition temperatures does not seem to be very meaningful at this stage.

Conclusions

The synchrotron SAXS scattering method was applied to study the order-disorder transition and micro-phase separation kinetics of a polyester-based segmented block copolymer. The material used in this work provides relatively high X-ray scattering intensity enabling the quantitative analysis of the data.

The structural changes which occur during the heating process were characterized with the one-dimensional correlation functions and interfacial parameters, such as interfacial thickness and Porod constant obtained from the Porod analysis, assuming linearly changing electron density at the interfacial region. The periodic structure observed from the correlation functions at low temperature disappeared above 150°C, which was melting transition temperature of the sample. At this temperature, a sharp decrease of the Porod constant was also observed.

Domain spacing increased slowly up to about 90°C, presumably due to the thermal expansion of the domains. The change rate of the domain spacing abruptly increased at about 90°C. This indicates that major structural changes occur well below the melting transition of the sample. The structural change occurring at above 90°C was also confirmed from the interfacial thickness. The interfacial thickness, which stays almost constant at low temperatures, starts to increase at about 90°C. This change might be due to dissolution of the thermally unstable hard domains and/or interdiffusion of the hard and soft segments in the interfacial regions.

The SAXS profiles were obtained during the isothermal micro-phase separation at various temperatures. They showed clearly the formation of the heterogeneous phase-separated structure from the initial homogeneous mixed state. The phase separation rate was found to be a sensitive function of the temperature.

The scattering peak position stayed constant during the entire period of the isothermal micro-phase separation process studied in this work. This behavior seems to be a characteristics of the phase separation of the segmented block copolymers, and it might be a manifestation of the extensive connectivity of the segments. It also means that the segments have to be stretched to take part in the phase separation process, even during the early stage of the micro-phase separation.

The experimental data was analyzed with the linearized Cahn-Hilliard diffusion equation assuming spinodal phase separation. Even though the scattering peak position was constant during the whole phase separation process, the exponential increase of the scattering intensity with time was observed only during the early stage. From the region of the exponential growth of the scattering intensity, amplification factors were obtained at various scattering vectors and temperatures. The diffusion coefficients obtained from the amplification factors were found to be negative, which is consistent with the spinodal phase separation. The spinodal temperature obtained by extrapolating the diffusion constant to zero was about 147°C. This type of analysis seems to indicate that the early stage of the micro-phase separation of segmented block copolymers might be interpreted with the linearized Cahn-Hilliard diffusion equation assuming spinodal mechanism.

The transition temperature was also obtained from the increase rate of the invariant. By extrapolating the invariant increase rate to zero, a transition temperature of about 145°C was obtained, which is comparable with the results obtained above. Due to the lack of a complete phase diagram for segmented block copolymers, further analysis on the exact nature of the transition temperatures obtained with two different methods appears to be unnecessary at this stage.

Acknowledgement

Synchrotron SAXS experiments at PLS were supported by MOST and POSCO in Korea. This work has been supported by the INHA University research program (code number 21071/2000).

References

1. H. F. Mark, N. M. Bikales, C. G. Overberger, and G. Menges, "Encyclopedia of Polymer Science and Engineering", 2nd ed., Vol. 13, John Wiley & Sons, New York, 1988.
2. I. Goodman, "Developments in block copolymers", Applied Science Publishers, London and New York, 1985.
3. G. Oertel, "Polyurethane Handbook", 2nd ed., Carl Hanser Verlag, New York, 1994.
4. C. Hepburn, "Polyurethane Elastomers", Elsevier Science, New York, 1992.
5. Y. Li, T. Gao, J. Liu, K. Linliu, C. R. Desper, and B. Chu, *Macromolecules*, **25**, 7365 (1992).
6. T. Hashimoto, K. Kowsaka, M. Shibayama, and H. Kawai, *Macromolecules*, **19**, 754 (1986).
7. P. Svoboda, J. Kressler, T. Chiba, T. Inoue, and H. W. Kammer, *Macromolecules*, **27**, 1154 (1994).
8. T. Hashimoto, *Macromolecules*, **20**, 465 (1987).
9. T. P. Russell and I. Chin, *Colloid & Polymer Science*, **272**, 1373 (1994).
10. K. Otake, H. Inomata, Y. Yagi, M. Konno, and S. Saito, *Polymer Communications*, **30**, 203 (1989).
11. R. Jenkins, R. W. Gould, and D. Gedcke, " Quantitative X-ray Spectrometry", 2nd ed., Marcel Dekker Inc., New York, 1995.
12. H. Yang, M. Shibayama, R. S. Stein, N. Shimizu, and T. Hashimoto, *Macromolecules*, **19**, 1667 (1986).
13. G. Floudas, S. Pispas, N. Hadjichristidis, T. Pakula, and I. Erukhimovich, *Macromolecules*, **29**, 4142 (1996).
14. J. G. Connell, R. W. Richards, and A. R. Rennie, *Polymer*, **32**, 2033 (1991).
15. H. S. Lee and T. Kyu, *Macromolecules*, **23**, 459 (1990).
16. B. Chu, T. Gao, Y. Li, J. Wang, C. R. Desper, and C. A. Byrne, *Macromolecules*, **25**, 5724 (1992).
17. W. C. Zin and R. J. Roe, *Macromolecules*, **17**, 183 (1984).
18. Y. Li, T. Gao, and B. Chu, *Macromolecules*, **25**, 1737 (1992).
19. T. K. Kwei, *Appl. Polym. Sci.*, **27**, 2891 (1982).
20. Y. Camberlin and J. P. Pascault, *J. Polym. Sci., Polym. Phys.*, **22**, 1835 (1984).
21. K. K. Chee and R. Farris, *Appl. Polym. Sci.*, **29**, 2529 (1984).
22. H. S. Lee, Y. K. Wang, W. J. MacKnight, and S. L. Hsu, *Macromolecules*, **21**, 270 (1988).
23. H. S. Lee and S. L. Hsu, *Macromolecules*, **22**, 1100 (1989).
24. J. W. Cahn, *Trans. TMS-AIME*, **242**, 166 (1968).
25. A. J. Ryan, *Polymer*, **31**, 707 (1990).
26. T. Hashimoto and T. Izumitani, *Macromolecules*, **26**, 3631 (1993).
27. M. J. Elwell, S. Mortimer, and A. J. Ryan, *Macromolecules*, **27**, 5428 (1994).
28. B. J. Park, S. Y. Rah, Y. J. Park, and K. B. Lee, *Rev. Sci. Instrum.*, **66**, 1722 (1995).
29. T. Hashimoto, K. Kowsaka, M. Shibayama, and S. Suehiro, *Macromolecules*, **19**, 750 (1986).
30. Z. Ophir and G. L. Wilkes, *J. Polym. Sci., Polym. Phys.*, **18**, 1469 (1980).
31. O. Glatter and O. Kratky, "Small Angle X-ray Scattering", Academic Press, London, 1982.
32. T. Pakula, K. Saijo, H. Kawai, and T. Hashimoto, *Macromolecules*, **18**, 1294 (1996).
33. J. D. Tanzer, C. R. Bartles, B. Crist, and W. W. Graessley, *Macromolecules*, **17**, 2702 (1984).
34. C. R. Bartles, B. Crist, and W. W. Graessley, *Macromolecules*, **17**, 2708 (1984).
35. H. S. Lee, S. R. Yoo, and S. W. Seo, *J. Polym. Sci., Polym Phys.*, **37**, 3233 (1999).
36. D. R. Paul and S. Newman, "Polymer Blends", Academic Press Inc., San Diego, 1978.
37. P. E. Gibson, J. W. C. Van Bogart, and S. L. Cooper, *J. Polym. Sci., Polym. Phys.*, **24**, 885 (1986).
38. G. L. Wikes and S. Abouzahr, *Macromolecules*, **7**, 355 (1974).
39. D. W. Van Krevelen, "Properties of Polymers", 3rd ed., Elsevier Science, New York, 1990.